Materials Today Communications 39 (2024) 108632

Contents lists available at ScienceDirect

Materials Today Communications

journal homepage: www.elsevier.com/locate/mtcomm

Parametric optimization of bio-inspired engineered sandwich core

Bianca Omede' *, Antonio Mattia Grande

Dipartimento di Scienze e Tecnologie Aerospaziali (DAER), Politecnico di Milano, Via La Masa, 34, Milano, 20156, Italy

ARTICLE INFO

Keywords:
Finite Element Analysis (FEA)
Bio-inspired structure
Complex PRoportional ASsessment (COPRAS)
Multi-objective optimization
Crashworthiness

ABSTRACT

The present study aims to design an efficient honeycomb cell structure for enhanced energy absorption. Elytra and bamboo bio-inspired parts were compared using a multi-criteria decision-making methodology (COPRAS) and finite element analysis (through Abaqus/CAE) to select the optimal candidate geometry for the study. A circular elytra-inspired geometry featuring four reinforcing cylinders was selected, demonstrating an increase in Specific Energy Absorption (SEA) of over 68% compared to a baseline geometry of the same mass. Structure optimization, aided by a genetic algorithm (NSGA-II), significantly improved crashworthiness parameters, presenting optimized values for design variables, This resulted in an increase in SEA by up to 94% and a 34% improvement in Crushing Force Efficiency (CFE) compared to a baseline geometry. The robust correlation between the algorithm and Finite Element Method (FEM) results highlights its usefulness for initial design, reducing computational demands. The research selects a circular elytra-inspired geometry featuring four reinforcing cylinders and showcasing the potential of multi-objective optimization algorithm in conjunction with FEM analysis in creating high-performance, lightweight structures for passive safety in aeronautics.

1. Introduction

The demand for lightweight structures with high energy absorption capacity has increased considerably in the past years in various engineering fields for which energy absorption applications are required (i.e., aerospace, transportation, nuclear reactors and civil engineering) [1]. For this reason, a number of energy absorbers with different structures has been tested and proposed with the aim of decreasing their weight while enhancing their safety and functional properties. Extensive research has been carried out that is finalized at the improvement of energy absorption of such structures due to direct axial impact [2].

Adhering to the principles of nature's design, biological entities have developed to be remarkably efficient and versatile, maximizing the utilization of all available materials and structures to thrive in challenging environments. Nature-inspired and biomimetic geometries can so possess a combination of lightweight properties and impact resistance, enabling them to endure external dynamic loads. This is achieved through captivating architectures that incorporate specialized design concepts, such as structural hierarchy, density gradients, and thin-walled tubular/cellular structures [3].

In aerospace, lightweight structures with low density, such as sandwich structures, play a significant role in ensuring crush resistance during impact and blast scenarios. Various types of lightweight sandwich structures, featuring cores like foams, lattices, and trusses, have been suggested for crashworthy applications. This is due to their ability to provide a remarkably low weight-to-area ratio while maintaining superior rigidity, strength, and capabilities for absorbing impact energy [4]. Thin-walled tubular structures of diverse shapes, from which the core may be made of, find extensive application as passive components for absorbing energy. Under severe loading conditions, these tubes effectively absorb and transform substantial amounts of kinetic energy, which stands out to be the most crucial parameter, into plastic strain energy [5].

Research has been carried out on the crash optimization of nested and multi-cell tubes, which represent preliminary efforts in exploring bioinspired designs incorporating a multi-cell concept. For example, Olabi et al. [6] delved into the effects of lateral impact on circular nested tube systems, demonstrating that optimized nested tubes exhibited a desirable force–deflection response when compared to standard tube systems. Nia and Chahardoli [7] optimized circular nested tube systems with varying height and thickness under quasi-static crushing conditions. San Ha et al. [8] conducted an investigation into the dynamic crushing behaviour of bio-inspired Hierarchical Multi-cell Square (BHMS) tubes, which were designed to mimic the gradient distribution of cell sizes found in biological structures such as bone and bamboo. The findings revealed that the BHMS tube exhibits a significantly greater potential for enhancing energy absorption compared to both the square tube and the conventional multi-cell square tube.

* Corresponding author.
E-mail addresses: bianca.omede@polimi.it (B. Omede'), antoniomattia.grande@polimi.it (A.M. Grande).

https://doi.org/10.1016/j.mtcomm.2024.108632
Received 11 December 2023; Received in revised form 29 February 2024; Accepted 13 March 2024
Available online 15 March 2024

Furthermore, several recent studies have focused on optimizing bio-inspired cellular-tubular designs for enhancing the energy absorption using genetic algorithms and multi-criteria decision making methodologies. Usta et al. [5] optimized tri-tubular nested and concentric circular tubes systems using a multi-objective optimization approach through the integration of genetic algorithm, response surface method, and Finite Element (FE) modelling under dynamic impact loading conditions, demonstrating that employing nested tubes, as opposed to single tubes with equivalent masses, can result in a reduction in the total weight of the vehicles. Meng et al. [9] used Non-dominated Sorting Genetic Algorithm II (NSGA-II) to identify the optimal design parameters, such as lattice cell size and shape, foam density and solid layer thickness, of bio-inspired sandwich Selective Laser Melting (SLM) printed structures with different core-arranged layered configurations. The results of the optimization process showed that bio-inspired sandwich structures have excellent mechanical properties and they are significantly lighter than traditional solid structures. San Ha et al. [10] utilized the COmplex PRoportional ASsessment (COPRAS) method to optimize the performance of bio-inspired tree-like forms in fractal multi-cell circular tubes designed for energy absorption. The numerical results demonstrated that the specific energy absorption increased proportionally with the fractal order, surpassing that of the conventional multi-cell circular tube. San Ha et al. [11] additionally suggested a parametric examination of a honeycomb sandwich panel inspired by the microstructure of a woodpecker's beak. This study aimed to explore the effects of wave amplitude, wave number, and core thickness on the energy absorption performance of the structures. The results indicated that a core with a larger wave number and amplitude exhibited higher Specific Energy Absorption (SEA), and an augmentation in core thickness led to an improvement in SEA.

Additive Manufacturing (AM) can significantly contribute to aeronautical passive safety with its reduced production costs and, above all, enabling greater design complexity [12]. A huge variety of bio-inspired structures have already been fabricated using 3D-printing technology based on stereolithography, inkjet printing, selective laser sintering, selective laser melting and fused deposition modelling [13]. Given the nature of the geometries and structures outlined in this paper, they appear to be well-suited for this specific manufacturing process. Among bio-inspired nested and multi-cell 3D printable geometries, structures inspired by the elytra of insects and the internal structure of bamboo show excellent energy absorption properties, as highlighted in San Ha and Guoxing work [1], especially when compared to conventional geometries.

Research towards structures inspired by the beetle elytron plate is of great importance. This structure is made of a trabecular sandwich with outer and inner thin-walled layers. The trabecular layer is composed of a network of interconnected hexagonal and cylindrical struts, which provide additional support and stability to the structure. Xiang and Du [14] and Yu et al. [15] showed that the honeycomb column structure exhibits excellent energy absorption properties, with a high specific energy absorption capacity and a stable deformation process, indicating an increase in specific energy absorption of even more than 107% if considering conventional crash boxes, such as in the case of Hao and Du's work [16]. Bamboo and horsetail structure have a similar unique design consisting of a tubular column with periodic nodes, containing also hollow multi-cell structures [1]. Bamboo structures have been mimicked by concentric circular tubes connected through differently-shaped bionic elements. Zou et al. [17], for bamboo-inspired structures, and Xiao et al. [18], for horsetail-inspired patterns, demonstrated that biomimetic methods could improve energy absorption performance under conditions of axial and lateral impact and bending. The numerical findings revealed a 124.8% enhancement in the load-bearing capacity of the biomimetic shell.

In the context of crashworthiness optimization, employing direct non-linear Finite Element Analysis (FEA) can be highly inefficient or even unfeasible. This is primarily due to the fact that iterative FEA during optimization typically demands extensive computational resources and carries a substantial risk of early simulation failure before achieving proper convergence. Consequently, surrogate models, also known as metamodels, are frequently utilized as a viable alternative to express the design criteria in terms of an explicit function of design variables prior to the optimization process [19]. This approach has demonstrated its effectiveness for a wide range of structural and crashworthiness applications [20–23].

In this research, the dynamic crushing response of two bio-inspired core cells in sandwich panels is investigated, mimicking the hierarchical structures found in the elytra of beetles and the internal structure of bamboo. The objective of this study is to design and optimize an efficient bio-inspired honeycomb cell, leveraging the opportunities provided by structural optimization through the implementation of numerical algorithms and finite element analysis. The ultimate goal is to enhance SEA, thereby contributing to the literature with an optimum under dynamic impact loading.

The paper is structured as follows: Section 2 introduces the FE framework and setup. In Section 3, the crashworthiness comparison of two different bio-inspired families (elytra and bamboo) is conducted using the COPRAS methodology. This process leads to the selection of the best candidate structure for subsequent optimization. Section 4 delves into the multi-objective optimization approach for the selected structure, integrating NSGA-II, the response surface method, and FE modelling under dynamic impact loading conditions. This follows a Design Of Experiment (DOE) approach. In Section 5, the results of the optimization are discussed, and finally, in Section 6, the conclusions are presented.

2. Finite element (FE) modelling

FE models of the different geometries for explicit dynamic simulations were developed using the non-linear FE code Abaqus/CAE-Explicit [24]. These models were used to predict the response of the tested structures subjected to a free-falling impinging mass [21]. The models were made up of the structure under study, a striker (i.e., the mass) and a base. The thin-wall structure was modelled by using 4 node shell continuum (S4R) elements with 5 integration points along the thickness direction of the element. Enhancement-based hourglass control was used to avoid artificial zero energy deformation modes and reduced integration was used to avoid volumetric locking. A mesh sensitivity analysis was conducted to obtain the convergence of the force–displacement curves to have a mesh-independent solution. Accordingly, the response of an elytra-inspired circular geometry facing four reinforcing cylinders (EC4, refer to Section 3.2.1 for the explanation of the structure's name) with different mesh sizes of 0.3 mm, 0.3 mm, 0.5 mm, 0.6 mm, 0.7 mm, 0.8 mm, 1 mm, 1.5 mm and 2 mm was examined. Fig. 2 shows the obtained force–displacement curves with different mesh sizes. It is clear that the shape of the force–displacement curve is almost similar when the mesh was smaller than 0.5 mm. To balance the computational time and result accuracy, the size of S4R elements is set to 0.5 mm for all the following investigations. The striker and the base were modelled as discrete rigid planar shell features. The former had only one allowable translational displacement and all other translational and rotational degrees of freedom were restrained to zero. The initial impact velocity of the striker on the structures was set to 10 m/s with a lumped mass of 200 kg, which were selected after having conducted analysis at various kinetic impact energies to establish sensible impact's conditions on the parts to be tested. The base was instead constrained with an encastre boundary condition. The contact algorithm used to simulate contact interaction between all components was the "general contact algorithm" [25]. This not only prevented interpenetration between the walls of the structures, but also simulated the friction between different parts of the model. The value of the tangential Coulomb friction coefficient for all

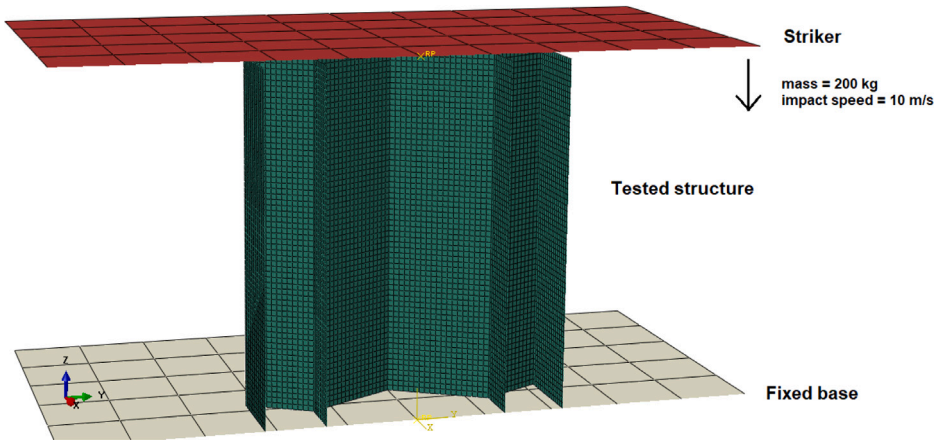

Fig. 1. FEM model setup.

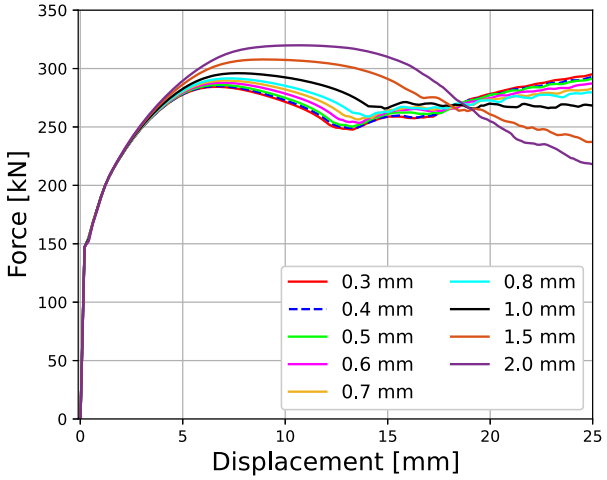

Fig. 2. Force–displacement curves for mesh sensitivity analysis on EC4, with varying mesh sizes.

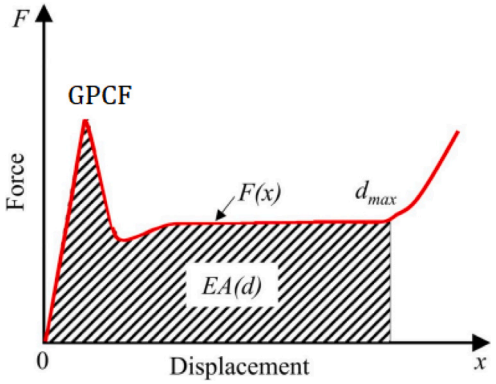

Fig. 3. Typical force–displacement curve [1].

contact surfaces was set at 0.2, while a normal pressure-overclosure hard contact was also accounted. FE analysis set-up is shown in Fig. 1 for the sake of clarity.

In order to obtain force–displacement diagrams, the load was measured off from the reaction force at the fixed base, resembling the principle on how load cells are used in actual physical tests, while the displacement was equal to the one of the striker. Structural material used was A36 steel (mild steel) [22]. The plastic material properties of A36 were characterized using the Johnson-Cook constitutive isotropic hardening model, which incorporates the effects of strain hardening, strain rate, and thermal softening. It is particularly applicable in situations where the strain rate varies significantly and the temperature changes due to thermal softening caused by plastic deformation.

3. Crashwortiness comparison of different bio-inspired geometries

3.1. Structural crashworthiness indices

The criteria for quantitatively evaluate the crashworthiness of different structures and thus assessing the effectiveness of their optimization are established by referencing the force–displacement profile of an energy absorber subjected to either crushing force or controlled displacement, as defined in the literature [1]. A representative force–displacement curve is illustrated in Fig. 3.

The parameters depicted in Fig. 3 are the axial crushing force *F(x)* as function of displacement *x* during the compression phase, the effective deformation distance d_{max}, the Global Peak Crushing Force (GPCF or F_{max}), that is the maximum crushing force during the whole crushing process (i.e., the maximum value of force in the force–displacement graph), the Energy Absorption (EA). Usually, four indicators are used to define crashworthiness performance [16]:

Energy absorption (EA): it is mainly used to evaluate an energy absorber's ability to dissipate crushing energy through plastic deformation, it is represented by the area under the force–displacement curve

$$EA(d) = \int_0^{d_{max}} F(x)dx \tag{1}$$

Specific Energy Absorption (SEA): it is defined as the ratio of the EA by a structure to its mass (M)

$$SEA(d) = \frac{EA(d)}{M} \tag{2}$$

SEA permits to compare energy-absorption performance of different materials and structures.

Mean crushing force (P_m): average compressive force exerted by the energy absorber over the total effective deformation, defined as:

$$P_m = \frac{EA(d)}{d_{max}} \tag{3}$$

Crush Force Efficiency (CFE): another indicator in energy absorption capacity. A higher value of CFE indicates a better loading uniformity: this means that when this value approaches unity, the energy-absorption mechanism experiences minimal changes in deceleration, which is beneficial for minimizing potential harm or damage to passengers or other payloads. It is defined as:

$$CFE = \frac{P_m}{F_{max}} \tag{4}$$

Table 1
Weightage setting for COPRAS methodology.

Selection	Number of comparison sets N = 3			W_j	w_j
criteria	1	2	3		
F_{max}	2	3		5	5/12 = 0.4167
EA	2		3	5	5/12 = 0.4167
CFE		1	1	2	2/12 = 0.1667
	Total Σ			G = 12	1

3.2. COPRAS methodology for a suitable geometry selection

In this study, the structure with the best crashworthiness performance under an axial impacting load was selected from the forty sectional configurations which will be later presented in terms of the aforementioned design criteria.

A method capable of assuming direct and proportional dependences of the significance and utility degree of the available alternatives under the presence of mutually conflicting criteria was used to proceed to the selection of the best available option. The chosen Multi-Criteria Decision Making (MCDM) process was the COmplex PRoportional ASsessment method (COPRAS) [26]. The selection of this method was based on its ease of use. The approach assumes direct and proportional dependencies between the significance and utility degree of available alternatives when dealing with mutually conflicting criteria. It considers the performance of alternatives across various criteria and their corresponding weights. The method determines the optimal decision by taking into account both the ideal and least preferred solutions. The COPRAS method has proven to be successful in addressing design selection problems not only in the fields of aeronautics and crashworthiness [21,22] but also others such as construction, project management, and economics [26].

COPRAS process is articulated in 7 steps:

*Step 1: Generation of an initial matrix **X** to map the alternatives to the selection criteria*

The initial matrix **X** can be expressed as follow:

$$X = [x_{ij}]_{mxn} = \begin{bmatrix} x_{11} & x_{12} & \cdots & x_{1n} \\ x_{21} & x_{22} & \cdots & x_{2n} \\ \vdots & \vdots & \ddots & \vdots \\ x_{m1} & x_{m2} & \cdots & x_{mn} \end{bmatrix} \quad (5)$$

where x_{ij} denotes the performance value of the ith alternative on the jth criterion, m is the number of compared alternatives (design concepts) and n is the number of design criteria (performance indicators).

*Step 2: Normalization of the decision matrix **R***

Since most design criteria do not have the same dimensions or units, selection could become hard. The easiest way to overcome this problem and have a better comparison between the selection criteria is to convert the initial matrix **X** to a non dimensionalize matrix **R**. The decision matrix **R** can be expressed as follow:

$$R = [r_{ij}]_{mxn} = \frac{x_{ij}}{\sum_{i=1}^{m} x_{ij}} \quad (6)$$

Step 3: Determination of individual weightages for different criteria

In order to compute the individual weightage w_j for each criteria, the following method should be followed:

- Compare two criteria at a time. Total comparison set is equal to $N = (n(n-1)/2)$, where n is the number of selection criteria
- Amongst the two criteria under comparison, a score of three (3) is assigned to the most important one, while the other is given a score of one (1). If the two criteria are of equal significance, a score of two (2) is assigned to both. This point shall be repeated for all the other comparison sets
- The total score obtained for each criteria is computed as

$$W_j = \sum_{i=1}^{m} N_{ij} \quad (7)$$

- A relative emphasis weighting factor, w_j, is obtained for each selection criteria by dividing the total score for each selection criteria W_j by the global total score given by

$$G = \sum_{i=1}^{m} W_{ij} \quad (8)$$

*Step 4: Determination of the weighted normalized decision matrix **D***

The weighted normalized decision matrix **D** can be expressed as follow:

$$D = [y_{ij}]_{mxn} = r_{ij} \times w_j \quad (9)$$

Step 5: Summation of beneficial and non-beneficial attributes

The normalized decision matrix consists of both beneficial and non-beneficial attributes for which, respectively, a high and a low value are desirable. These sums can be expressed as follow, respectively:

$$S_{+i} = \sum_{i=1}^{m} y_{+ij} \quad (10)$$

$$S_{-i} = \sum_{i=1}^{m} y_{-ij} \quad (11)$$

The greater the value of S_{+i} and the lower the value of S_{-i}, the better is the design concept.

Step 6: Computation of relative significance of priority Q

The design concepts are evaluated and ranked according to their relative significance Q_i. A higher Q_i value indicates a higher priority for the design concept. This parameter represents the level of satisfaction achieved by each concept. The design concept with the highest relative significance Q_{max} is considered the optimal choice for the concept selection decision. The relative significance of priority Q_i can be expressed as follow:

$$Q_i = S_{+i} + \frac{S_{-min} \sum_{i=1}^{m} S_{-i}}{S_{-i} \sum_{i=1}^{m} (S_{-min}/S_{-i})} \quad (12)$$

where S_{-min} is the minimum value of S_{-i}.

Step 7: Determination of the quantitative utility U

The ranking of the alternatives is finalized by incorporating quantitative utility values, which can be expressed using the following formula:

$$U_i = \frac{Q_i}{Q_{max}} \times 100\% \quad (13)$$

The performance of a design alternative is determined by the degree of its quantitative utility: a higher degree U_i indicates better performance. The design alternative with a utility value of 100% is considered the best design according to the evaluation method used. The alternatives are therefore ranked based on their quantitative utility. The design alternative with a ranking of 100% holds the top position, followed by the one with the second-highest U_i value, and so forth.

Regarding the design criteria considered, the absorbed energy (EA) and crushing force efficiency (CFE) were accounted as beneficial attributes as their maximization is regarded positively, and the compression peak force (F_{max}) was accounted as non-beneficial, since its minimization is sought to reduce accelerations transmitted to possible payload. The weightage of the different criteria was performed by completing Table 1. It was assumed that the maximum force and the absorbed energy were equally important, while the CFE was relatively less significant.

3.2.1. Configuration of selected geometries

As previously identified in Section 1, the most promising geometries for specific energy absorption appeared to be inspired by the internal structure of bamboo and the elytra of insects, whose microstructures are shown in Figs. 4(a) and 4(b), respectively. Examples of available bio-inspired designs found in literature and which inspired the present work are illustrated in Fig. 5.

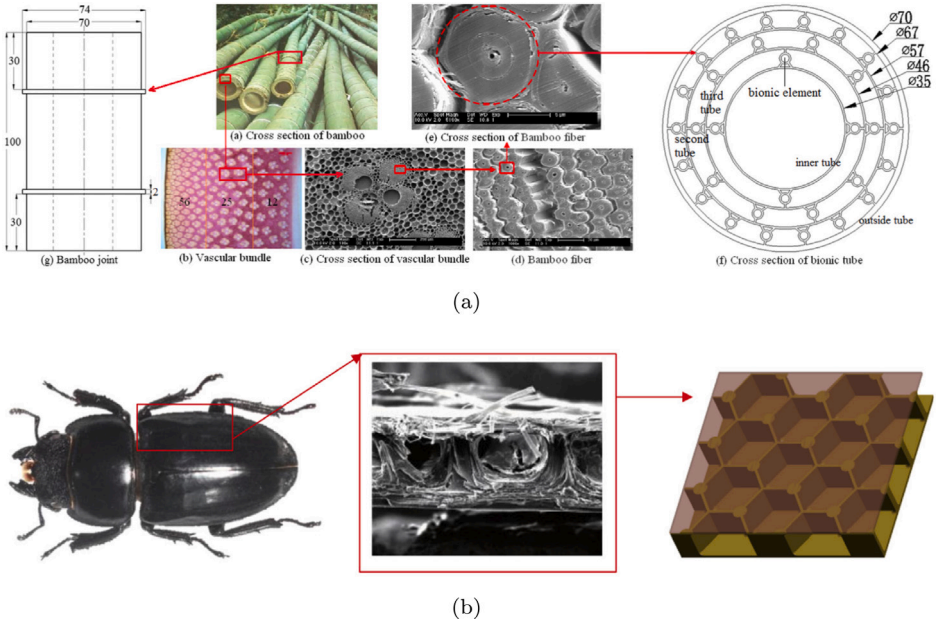

Fig. 4. Microstructures and bionic designs inspired by (a) bamboo [17] and (b) beetle forewing [27].

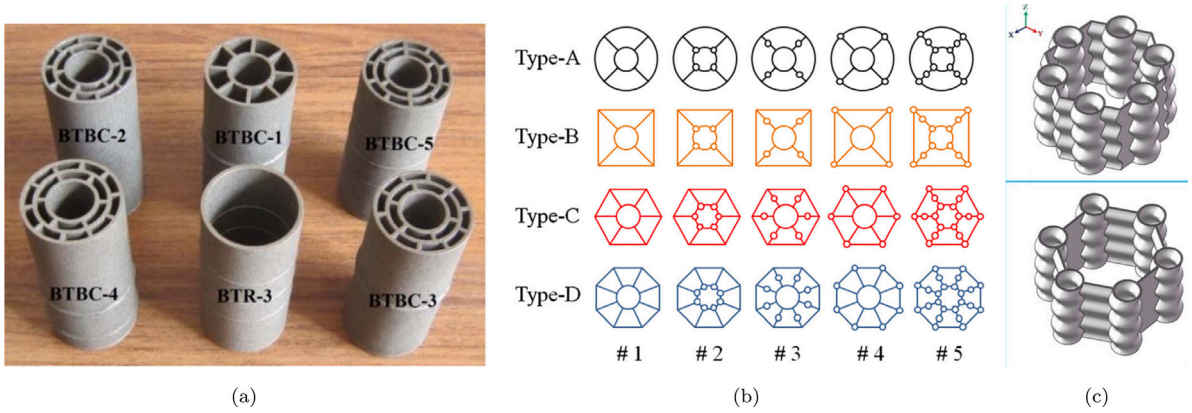

Fig. 5. (a) 3D-printed bamboo-inspired tubes with simplified bionic elements [28], (b) Cross-sectional configurations of the bionic multi-cells tubular thin-walled structures [29], (c) End-trabecular and middle-trabeculare beetle elytron inspired crash boxes [15].

For this reason, four types of geometries have been chosen for a preliminary research on the structure to be further optimized: a bamboo-inspired one, with circular walls and ribs between concentric features, a bamboo-inspired one, with linear walls (so having a polygonal external shape) and ribs connecting the polygon's edges an elytra-inspired one, with a circular main structure and a number of reinforcing cylinders and lastly an elytra-inspired one, with linear walls of the main structure (so having a polygonal external shape) and reinforcing cylinders placed with their center corresponding to the polygon's edges.

In comparison to existing literature, in the investigation of structures with high energy-absorption capabilities, the variation in the number of concentric features within a honeycomb panel cell, the cell shape, and the number of sides or elements incorporated appears to be of interest. Regarding the undulation of the cell walls, as exemplified in Fig. 5(c), this parameter was subsequently included in the optimization explained in Section 4 performed with NSGA-II in order to find optimal design variables, after the best candidate geometry is selected with COPRAS. It was decided to set the maximum external dimensions and height of all the structures that were subsequently tested and optimized at 50 mm each, in order to be able to meaningfully compare the results. The force–displacement diagrams and the corresponding values of absorbed energy have been calculated up to a compression deformation length of 20 mm, which is 40% of the height of the structure. Considering the selected kinetic energy conditions, in fact, all the simulations for the two families prevented both material rebound effects and impacting mass back-bouncing within this compression distance.

To proceed with the use of the COPRAS methodology, as reported in Ref. [22], the structures were supposed to possess equal masses.

To avoid including and testing components that possessed undesirable characteristics, such as excessive stubbiness or excessively thin walls, the decision was made to proceed with the selection of the best geometry for both families separately. The simulations performed with geometries coming from the two different families were nonetheless conducted with identical boundary conditions and imposed loads, in order to ensure comparability of obtained results. For the elytra-inspired family of structures, considering fixed values for the maximum outer circumference and the height, geometric parameters that could be varied were the radius and number of reinforcing cylinders, as well as the thicknesses of the structure walls. By arbitrarily setting the radius of the reinforcing cylinders to 4 mm, a total of ten possible geometries had been identified for this family: five with a circular base and five with a polygonal base, each having 4/6/8/10/12 reinforcing

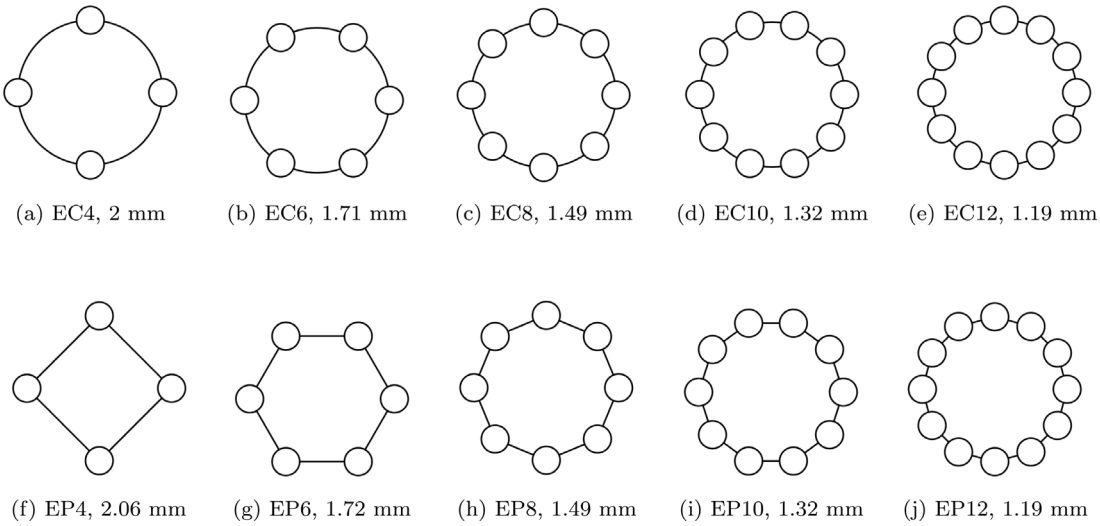

Fig. 6. Sectional configurations and thicknesses of elytra family geometries.

Table 2
Bamboo family wall thickness (WT) data.

	WT [mm]		WT [mm]		WT [mm]		WT [mm]		WT [mm]		WT [mm]
BC4_2	2.35	BC4_3	1.64	BC4_4	1.26	BP4_2	2.58	BP4_3	1.80	BP4_4	1.39
BC6_2	2.20	BC6_3	1.56	BC6_4	1.21	BP6_2	2.29	BP6_3	1.63	BP6_4	1.26
BC8_2	2.06	BC8_3	1.49	BC8_4	1.17	BP8_2	2.11	BP8_3	1.53	BP8_4	1.2
BC10_2	1.95	BC10_3	1.43	BC10_4	1.13	BP10_2	1.9	BP10_3	1.45	BP10_4	1.16
BC12_2	1.84	BC12_3	1.37	BC12_4	1.10	BP12_2	1.8	BP12_3	1.39	BP12_4	1.11

cylinders. Diagrams illustrating the various geometries and displaying the corresponding wall thicknesses are shown in Fig. 6. For the bamboo-inspired family structures, considering fixed values for the maximum outer circumference and the height, geometric parameters that could be varied were the radius and number of the various concentric features, the number of reinforcing ribs, as well as the thicknesses of the structure walls. By arbitrarily setting the radius of most inner feature to 15 mm, a total of thirty possible geometries had been identified for this family: fifteen with a circular base and fifteen with a polygonal base, each having 4/6/8/10/12 ribs combined with 2/3/4 concentric features. Fig. 7 provides examples of the created geometries with 4 reinforcing ribs and/or 4 edges in the case of the polygonal base. For the other structures, data regarding wall thickness are summarized in Table 2. For citation convenience, the geometries discussed in this section and hereafter follow a specific naming rule: they are denoted by two letters, where the first indicates the family from which the structure is inspired (e.g., 'E' for elytra and 'B' for bamboo), while the second letter indicates the shape of the base of the structure (e.g., 'C' for cylindrical and 'P' for polygonal). Following the two letters, a number is placed, indicating the radius of the reinforcing cylinders in the case of elytra-inspired structures and the number of ribs in the case of the bamboo ones. For structures from the latter family, an additional second number is added, indicating the number of concentric features. The thickness of the walls, equal for both the main structure and the reinforcing cylinders in case of the elytra-inspired geometry and the ribs in case of the bamboo-inspired geometry, has been varied in such a way that the structures would have reached arbitrarily selected target masses of 157 g and 268 g, respectively.

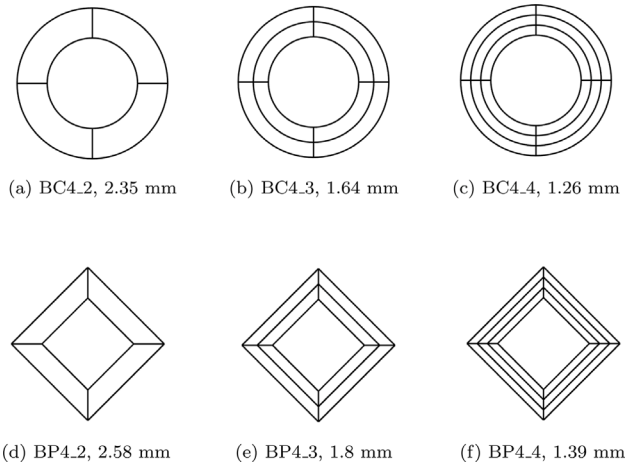

Fig. 7. Sectional configurations and thicknesses examples of bamboo family geometries.

3.2.2. Results of the COPRAS approach

The crashing responses of the forty tested structures are so reported and analysed. Fig. 8 presents the force–displacement diagrams obtained from the numerical tests conducted for the elytra family.

Tables 3 and 4 show the results obtained using the COPRAS approach for the elytra-inspired structures. They are reported exchanging

Table 3
Decision matrix (elytra family).

Section	F_{max} [kN]	EA [kJ]	CFE [–]
EC4	285.22	5.14	0.8671
EC6	301.03	4.40	0.6881
EC8	286.42	5.12	0.6469
EC10	281.77	3.63	0.6035
EC12	281.22	3.43	0.5679
EP4	282.37	4.69	0.7922
EP6	285.47	4.29	0.7067
EP8	284.28	3.95	0.6539
EP10	282.33	3.65	0.6065
EP12	281.20	3.43	0.5684

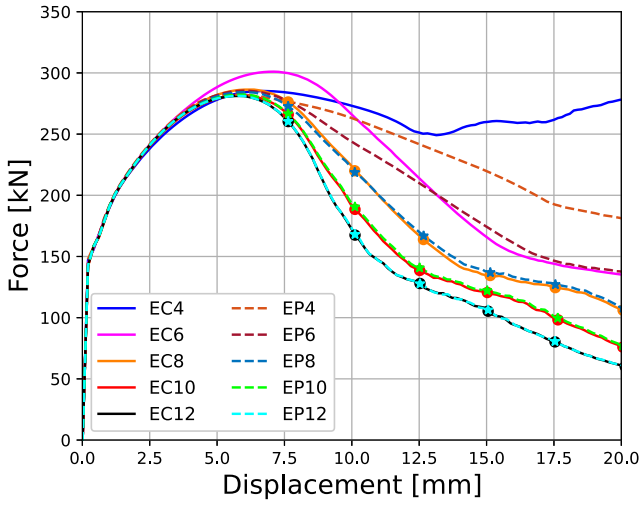

Fig. 8. Force–displacement diagram from elytra family simulations.

Table 4
COPRAS results of elytra family.

Section	S_-	S_+	Q_i	U_i	Rank
EC4	0.0417	0.0728	0.1145	100.00%	1
EC6	0.0440	0.0610	0.1005	87.80%	5
EC8	0.0419	0.0672	0.1087	94.93%	3
EC10	0.0412	0.0512	0.0934	81.58%	8
EC12	0.0411	0.0484	0.0906	79.17%	10
EP4	0.0413	0.0666	0.1086	94.94%	2
EP6	0.0417	0.0604	0.1020	89.16%	4
EP8	0.0415	0.0557	0.0975	85.17%	6
EP10	0.0413	0.0515	0.0936	81.76%	7
EP12	0.0411	0.0484	0.0906	79.20%	9

the rows with the columns compared to the original notation for the sake of convenience in representation.

The selected shape for designing an efficient energy absorber, chosen from the various possibilities offered by this family, was the circular-based geometry with 4 reinforcing cylinders (EC4), which was followed by the corresponding polygonal-based one (EP4).

Figs. 9(a)–9(c) instead show force–displacement diagrams obtained from the numerical tests conducted for the bamboo family.

Tables 5 and 6 show the results obtained using the COPRAS approach for the bamboo-inspired structures. They are reported exchanging the rows with the columns compared to the original notation for the sake of convenience in representation.

The selected shape for designing an efficient energy absorber, chosen from the various possibilities offered by this family was, in this case, the polygonal-based geometry with 8 ribs and 4 concentric features (BP8_4).

The deformation modes exhibited by some structures investigated with the COPRAS methodology are reported as examples in Fig. 10. EC4 and BP8_4 are selected as they emerged as the best candidates through the COPRAS method, while EP8 and BC4_4 are provided as significant examples. Overall, the collapse behaviour of these structures can be categorized into two main deformation modes: global buckling mode [8] and axisymmetric mode [30]. In global buckling mode, which is mainly experienced by the elytra-inspired parts, folding deformation occurs with localized buckling, resulting in walls exhibiting larger folding wavelengths compared to the other modes. The sole exception appears to be EC4, which exhibits a progressive mode of deformation. This mode is characterized by the gradual folding at one end or another position of the component, resulting in the generation of regular lobes in its walls and, consequently, in a reduction of fluctuation in the crushing force experienced by the structure. In axisymmetric mode, instead mainly experienced by the bamboo-inspired structures, an object or structure undergoes symmetric changes around an axis. In other words, the deformation pattern remains consistent as the object is rotated around its axis. This mode of deformation is often observed in symmetrically shaped objects subjected to axial loading or pressure, and to quite short shells.

Table 5
Decision matrix (bamboo family).

Section	F_{max} [kN]	EA [kJ]	CFE [–]
BC4_2	471.02	7.96	0.8234
BC6_2	540.95	8.86	0.8101
BC8_2	600.07	9.72	0.7449
BC10_2	633.07	9.93	0.6793
BC12_2	645.96	9.93	0.6659
BP4_2	520.36	9.16	0.8690
BP6_2	530.47	9.53	0.8933
BP8_2	571.27	9.93	0.7535
BP10_2	613.86	9.93	0.7786
BP12_2	629.55	9.93	0.7585
BC4_3	450.78	7.23	0.7888
BC6_3	469.81	7.85	0.8199
BC8_3	544.06	8.69	0.7976
BC10_3	605.02	9.51	0.5019
BC12_3	637.39	9.92	0.6785
BP4_3	392.82	6.99	0.8546
BP6_3	415.20	7.63	0.8869
BP8_3	461.33	8.48	0.8979
BP10_3	533.23	9.36	0.8752
BP12_3	609.71	9.93	0.7849
BC4_4	376.64	6.36	0.8137
BC6_4	400.72	7.01	0.8496
BC8_4	448.06	7.75	0.8494
BC10_4	505.94	8.86	0.8385
BC12_4	578.03	9.46	0.8293
BP4_4	364.34	5.77	0.7603
BP6_4	370.66	6.44	0.8352
BP8_4	400.37	7.40	0.8983
BP10_4	483.58	8.35	0.8520
BP12_4	544.91	9.23	0.8481

Table 6
COPRAS results of bamboo family.

Section	S_-	S_+	Q_i	U_i	Rank
BC4_2	0.0128	0.0186	0.0332	93.78%	17
BC6_2	0.0147	0.0200	0.0327	92.34%	22
BC8_2	0.0163	0.0209	0.0324	91.49%	24
BC10_2	0.0172	0.0208	0.0317	89.46%	27
BC12_2	0.0175	0.0207	0.0314	88.59%	29
BP4_2	0.0141	0.0209	0.0341	96.30%	10
BP6_2	0.0144	0.0216	0.0346	97.73%	6
BP8_2	0.0155	0.0213	0.0334	94.22%	15
BP10_2	0.0167	0.0215	0.0327	92.36%	21
BP12_2	0.0171	0.0214	0.0323	91.18%	25
BC4_3	0.0122	0.0172	0.0325	91.65%	23
BC6_3	0.0128	0.0184	0.0331	93.35%	18
BC8_3	0.0148	0.0196	0.0323	91.14%	26
BC10_3	0.0164	0.0189	0.0303	85.50%	30
BC12_3	0.0173	0.0208	0.0316	89.19%	28
BP4_3	0.0107	0.0173	0.0348	98.17%	5
BP6_3	0.0113	0.0185	0.0351	98.97%	2
BP8_3	0.0125	0.0200	0.0349	99.07%	3
BP10_3	0.0145	0.0213	0.0342	98.51%	9
BP12_3	0.0166	0.0215	0.0328	96.43%	20
BC4_4	0.0102	0.0160	0.0342	92.68%	8
BC6_4	0.0109	0.0173	0.0345	96.62%	7
BC8_4	0.0122	0.0185	0.0338	95.50%	11
BC10_4	0.0137	0.0197	0.0333	94.00%	16
BC12_4	0.0157	0.0211	0.0320	93.16%	19
BP4_4	0.0099	0.0146	0.0335	94.65%	13
BP6_4	0.0101	0.0162	0.0348	98.26%	4
BP8_4	0.0109	0.0182	0.0354	100.00%	1
BP10_4	0.0131	0.0195	0.0337	95.10%	12
BP12_4	0.0148	0.0208	0.0335	94.87%	14

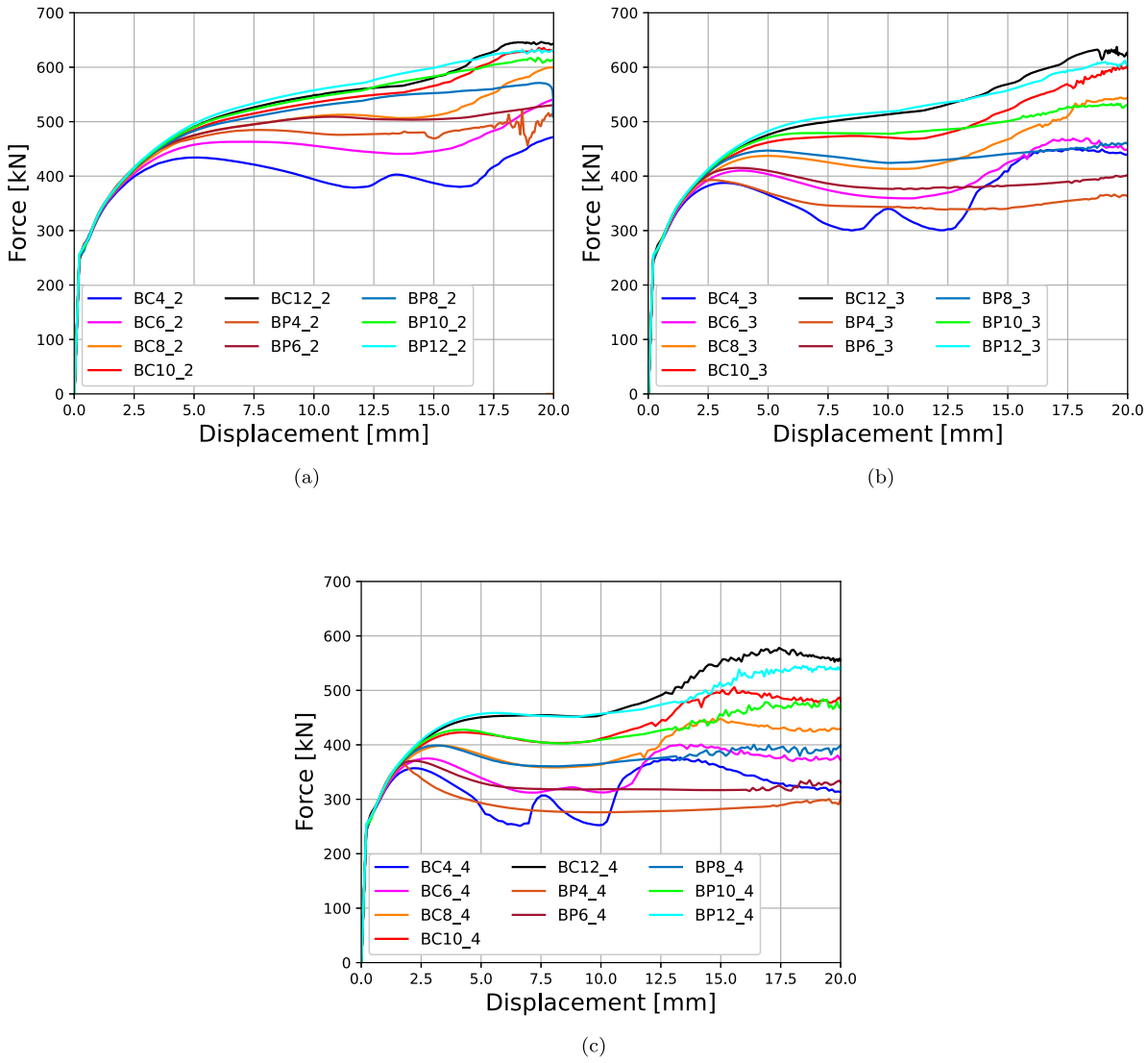

Fig. 9. Force–displacement diagrams from bamboo family simulations: (a) 2 concentric features, (b) 3 concentric features, (c) 4 concentric features.

Table 7
SEA comparison.

Geometry	SEA [J/g]	SEA reference cylinder [J/g]	% variation
EC4	32.65	19.38	68.47%
BP8_4	27.58	28.6	−3.56%

3.3. Selection for the optimal bio-inspired structure

As it can be observed from the obtained results, the candidate geometries for the subsequent optimization phase were EC4 and BP8_4. SEA proved to be the discriminating parameter in selecting the optimal geometry. Obtained SEA values are shown in Table 7. This table also reports reference cylinder's SEA values, which were computed through analogous simulation of two basic reference geometries. These reference cylinders are simple hollow metallic cylinders, which maintained the height and a constant diameter fixed to 50 mm while altering the wall thickness in order to reach, respectively, masses of 157 and 268 g. Force–displacement diagrams of reference cylinders compared to their respective selected geometries are shown in Figs. 11(a) and 11(b).

From Table 7 and Figs. 11(a) and 11(b), it is immediately evident that the best candidate is the EC4 geometry. It not only exhibited a higher SEA compared to EP8_4, but there was also a 68.4% increase in SEA compared to the reference base geometry, while the corresponding bamboo family member showed decreased performance in this regard. Furthermore, the EC4 has a significantly lower mass compared to the EP8_4, which is a crucial factor to be considered in designing lightweight structures in the aerospace field. The EC4 geometry was, therefore, chosen for the subsequent optimization phase, which involved optimizing the geometry by varying the thicknesses of the walls and cylinders, the radii of the cylinders, and the shape of the leading line of deformation along the height of the structure.

4. Crashworthiness optimization of the selected structure

According to the aforementioned comparative analyses, structure EC4, a circular elytron inspired geometry featuring four reinforcing cylinders, performs best under multicriteria and axial impacting loading case. Thus, a multi-objective optimization was carried out to find the best possible design.

Crashworthiness optimization typically involves conducting numerous nonlinear finite element simulations. Surrogate modelling has seen widespread usage as an efficient method to tackle this problem. A Design of Experiment (DOE) has been a widely-used technique for structural optimization in an initial design phase, since experimental design plays a critical role in optimizing production processes in science and engineering. It can lead to reduced variability, better adherence

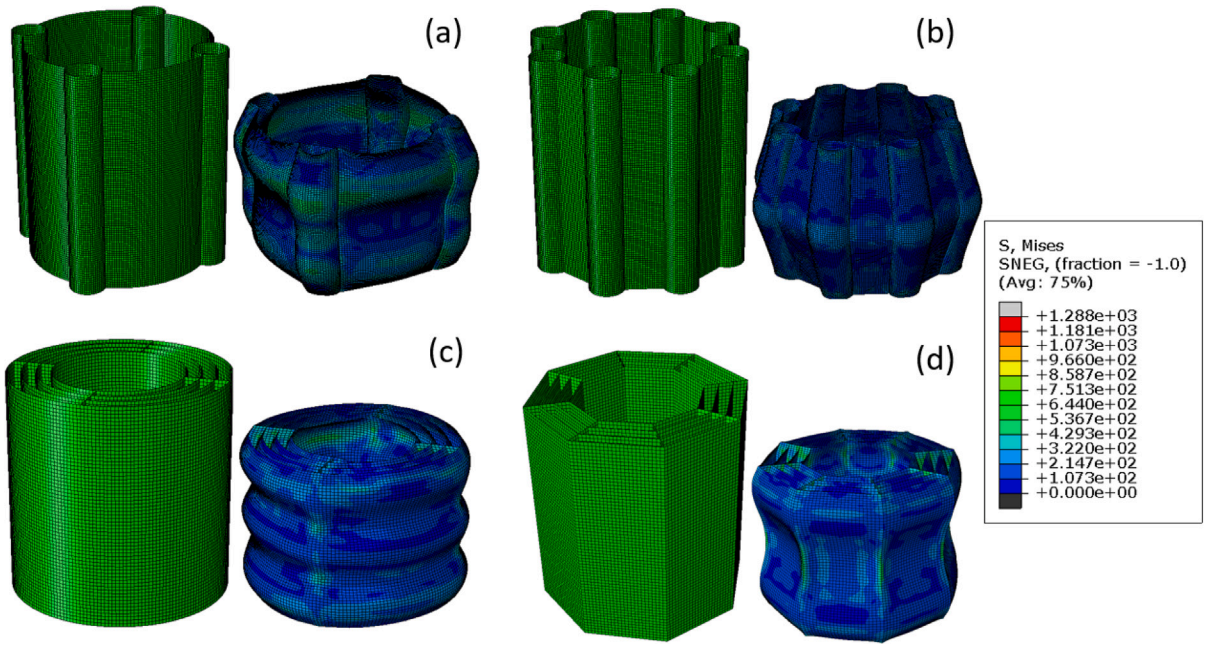

Fig. 10. Undeformed and deformed shapes of structures investigated with the COPRAS methodology: (a) EC4, (b) EP8, (c) BC4_4, (d) Bp8_4.

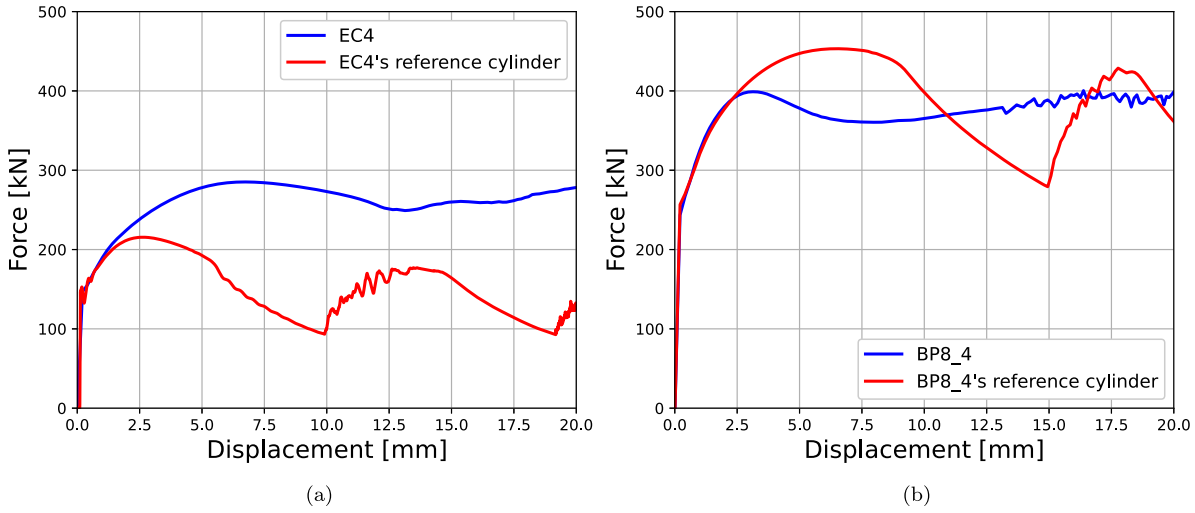

Fig. 11. Force–displacement graph comparison with reference cylinders: (a) U-F elytra comparison, (b) U-F bamboo comparison.

to target requirements, shorter development times, and lower overall costs if performed during the early stages of process development [31]. In this work, a response surface methodology approach was utilized. DOE approach consists in the following four steps: (1) Pre-experimental planning, (2) Choice of experimental design, (3) Conduction of the experiment, (4) Data analysis, model creation and validation. In the following paragraphs, each phase will be reviewed in more details.

4.1. Pre-experimental planning

The first step of the multi-objective optimization consisted in the identification of the response variables and of the geometrical factors with their ranges. The geometric design factors are the variables that were varied during the experiment and are thus were regarded as input factors affecting the system's performance. In this case, the response variables of interest were the maximum crushing force (GPCF or F_{max}), which was meant to be minimized because excessive impact force can result in significant deceleration, which could lead to severe injuries or even fatalities for the occupants, and the specific energy absorption (SEA), which was instead meant to be maximized, as the primary goal for an energy absorber is to maximize its energy absorption capacity [32].

The selected design variables, instead representing geometrical parameters varied to create diverse geometries, include walls thickness (t_w) in the range of 1 to 2.5 mm, reinforcing cylinders' thickness (t_c) in the range of 1 to 2.5 mm, radius of reinforcing cylinders (r) within 2.5 to 6 mm (with the external maximum diameter fixed, consequently influencing the main feature's diameter change) and a parameter of the leading line of deformations. Regarding this last variable, according to some studies [15], mechanical properties of a crash box can be adjusted to meet diverse engineering requirements by modifying the amplitude of the deformation lines. These results inspire the application of bionic structures based on beetle elytra and the utilization of new buffering structures to alleviate the detrimental effects of collision events and enhance crashworthiness performances. A sine wave deformation line of the form $Z = A\ sin(0.3 \times X)$ was implemented along the height of the structure to investigate these effects. Here, A is a parameter

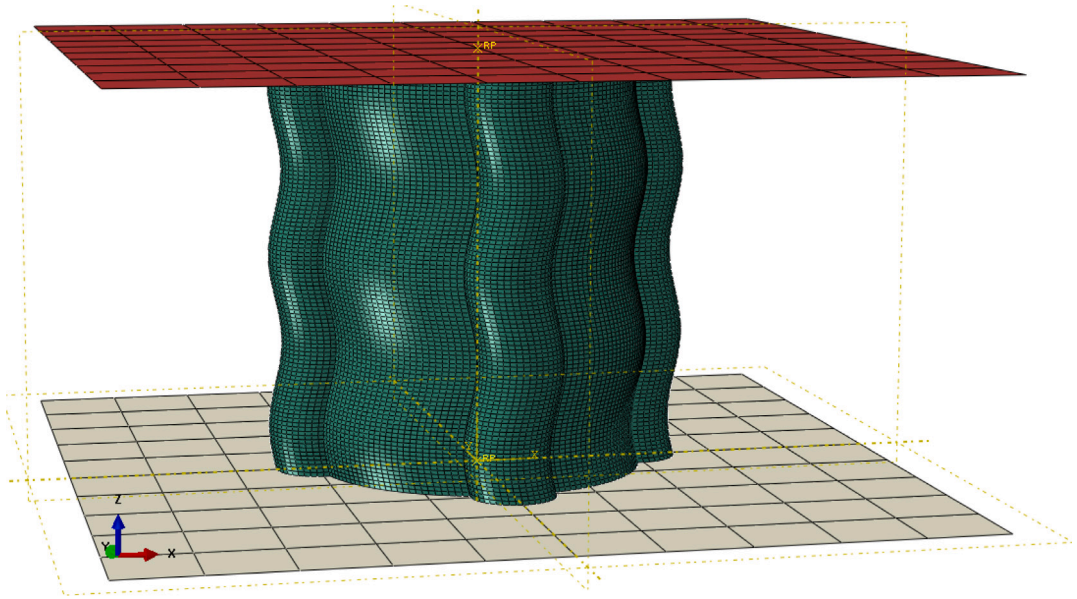

Fig. 12. Structure example obtained through OLHS parameters.

that regulates the amplitude (ranging from 0 to 1.5) of the sinusoidal function, while the periodicity is kept constant with a parameter equal to 0.3.

In conclusion, this study dealt with 2 response variables and 4 design variables, whose ranges were selected according to possible manufacturing (e.g., the lower limits for the thicknesses), geometrical (e.g., for A) and common-sense limits. The mathematical formulation of the optimization problem can be stated as Eq. (14):

$$\begin{cases} \min & \{F_{max}(t_w, t_c, r, A), -SEA(t_w, t_c, r, A)\} \\ \text{s.t.} & 1.0 \le t_w, t_c \le 2.5 \\ & 2.5 \le r \le 6.0 \\ & 0.0 \le A \le 1.5 \end{cases} \tag{14}$$

4.2. Choice of experimental design

The Optimal Latin Hypercube Sampling (OLHS) [21] is an advanced sampling technique used to select an optimized set of points within a Latin hypercube. It is a variant of the Latin Hypercube Sampling (LHD), but it aims to further improve the coverage and efficiency of exploring the parameter space. OLHS was employed to generate 50 training points, which were tested in the next phase of the DOE.

4.3. Conduction of the experiment

After the DOE test points had been selected, the configurations corresponding to sampled design variables were simulated through computational experiments using ABAQUS/CAE Explicit Solver. Simulations were performed following the same procedures explained in Section 2. S4R elements with a mesh size of 0.5 mm were selected after a mesh sensitivity analysis, according to Fig. 2. Fig. 12 shows an example of a structure created according to the parameters sampled with OLHS. The force–displacement graphs and mass properties were saved for each simulation conducted, thus permitting to compute the desired values of SEA and F_{max}.

4.4. Data analysis, model creation and validation

Once simulation data had been collected, the next step involved constructing a regression model to analyse the sample data. This model aimed to fit the data to reveal the connection between a response variable and the independent geometric factors. In order to verify the model's robustness and applicability, ensuring a robust alignment between the data obtained from the experiments and the data derived from regression, two parameters had to be computed and checked: the relative error and the value assumed by the coefficient of determination [33], which is defined as:

$$R^2 = 1 - \frac{\sum_{i=1}^{N} (z_i - \hat{y}_i)^2}{\sum_{i=1}^{N} (\hat{y}_i - \bar{z})^2} \tag{15}$$

This parameter falls within the range of 0 to 1, and it serves as an indicator of how effectively a statistical model can forecast an outcome. In this scale, a value of 1 signifies an impeccable match with the available data. In Eq. (15), $\bar{z}$ is defined as the mean value of the simulated response z, while $\hat{y}_i$ is the predicted one.

In this case, two regression models were needed: one for the maximum crushing force and one for the specific energy absorption.

Subsequently, Non-dominated Sorting Genetic Algorithm (NSGA-II) [34] was employed within the framework of multi-objective optimization to identify a Pareto-Optimal (PO) front representing the best and optimal solutions. It was chosen because it possesses the lowest possible computational complexity achievable with any non-dominated sorting approach, which is equal to $O(M N^2)$, where M is the number of objectives and N is the population size, and because it has proven to be effective in addressing crashworthiness optimization design problems of energy-absorbing structures [32,35]. Two performance metrics were used to assess the algorithm's performance and correct functioning: the hypervolume [36] and the running performance metric [37].

5. Results and discussion of the crashworthiness optimization

The regression model employed for the DOE points used a third-degree polynomial for polynomial features for both parameters. The model's maximum relative error R_e was found to be 1.9% for specific energy absorption and 1.7% for the maximum force regression models. Additionally, the coefficient of determination R^2 values were, respectively, 0.9980 and 0.9995. The regression model was then employed within the context of multi-objective optimization. The primary objective was to identify optimal configurations concerning both response variables. As illustrated in Fig. 13(a), the Pareto-Optimal front, indicative of non-dominated solutions, is positioned below and to the left of the DOE points. This position stands for the achievement of

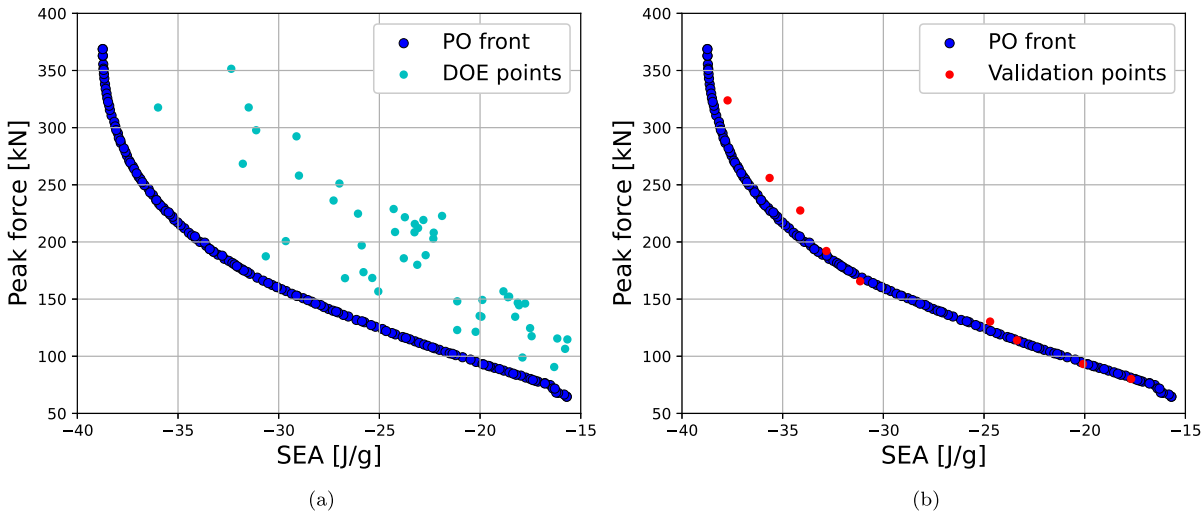

Fig. 13. (a) Pareto-Optimal front and DOE simulation points, (b) PO front and validation points.

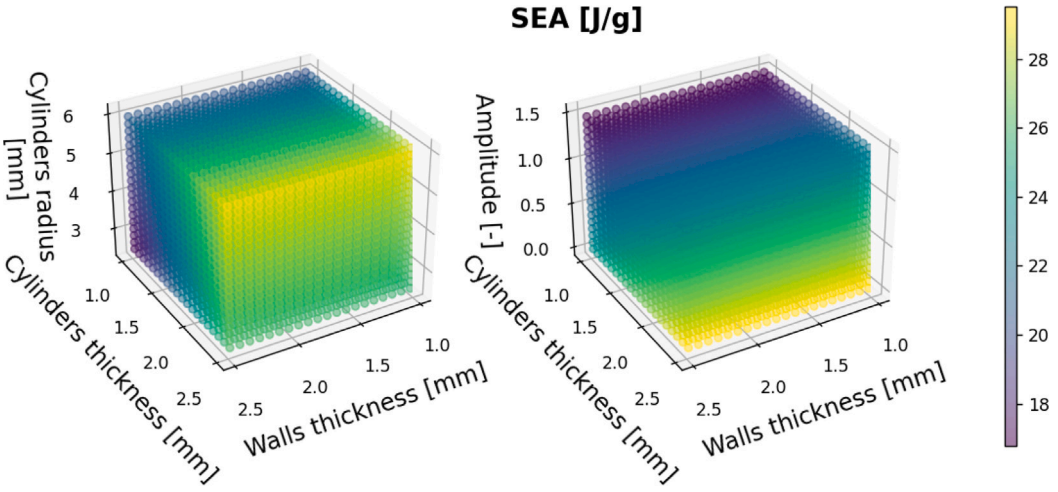

Fig. 14. Volume visualization of the specific energy absorption as predicted from the regression model.

configurations that minimize both the maximum force and the negation of the SEA (i.e., maximization of the SEA).

In order to ensure the utmost precision of the complete model, some validation points were randomly selected among the PO font points. These validation points serve the primary purpose of showcasing the accuracy of the derived outcomes, demonstrating that the results obtained through fitting and optimization exhibit a genuine correspondence when the same conditions are numerically simulated. The geometric parameters pertaining to the validation points were consequently employed to recreate structures tested in Abaqus/CAE, yielding a commendable predictive capability of the model, as evident in Fig. 13(b).

In order to comprehend which optimal design parameters had to be selected for finalizing the choice of an optimized geometry, it was useful to depict the parameters associated with the solutions of the PO front predicted by the multi-objective optimization model (refer to Figs. 14 and 15). These solutions are non-dominated and thus represent the most favourable choices considering the optimization of both response variables.

These two images are clearly quite similar, and it can be easily observed that high values of SEA, which should be maximized, correspond to high values of maximum force, which should be instead minimized.

As evident from these scatter diagrams, pursuing higher values of cylinders' radius and thickness is favourable for enhancing specific energy absorption, while walls' thickness and amplitude parameter are almost set completely to the same low range values for all configurations. However, if the primary goal is to minimize the peak force transmitted to occupants during an impact, the emphasis shifts to higher values of amplitude parameters and lower values of cylinder thickness and radius. In both cases, it is worth noting that the optimal value of the primary structure's wall thickness is very small.

While the Pareto set offers numerous potential design solutions during the initial design phase, a final decision needed to be made on the most desirable solution within the Pareto set. Regarding the selection of this point, there are several aspects to consider. A first approach was to choose the two configurations that maximize the SEA and minimize the peak force, and that are referred as, respectively, *Configuration 1* and *Configuration 2* in Fig. 16.

Alternatively, an optimal solution, referred to as *"Knee Point" (KP) configuration*, is often determined using the "minimum distance selection method" (TMDSM) [38]. This method focuses on quantifying the distance between solutions in the Pareto set and a reference point, that is called utopia point and it is determined by the optimal values of each individual objective (i.e., the ideal point), which are normally

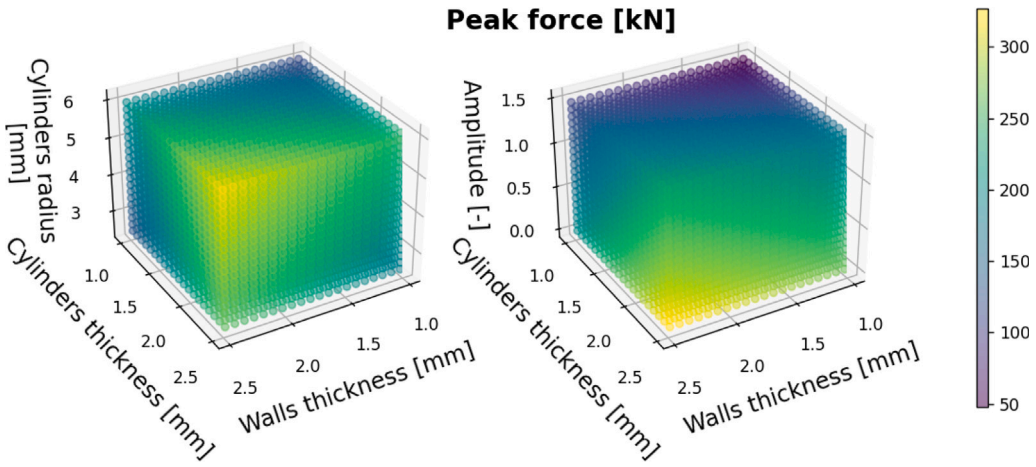

Fig. 15. Volume visualization of maximum peak force as predicted from the regression model.

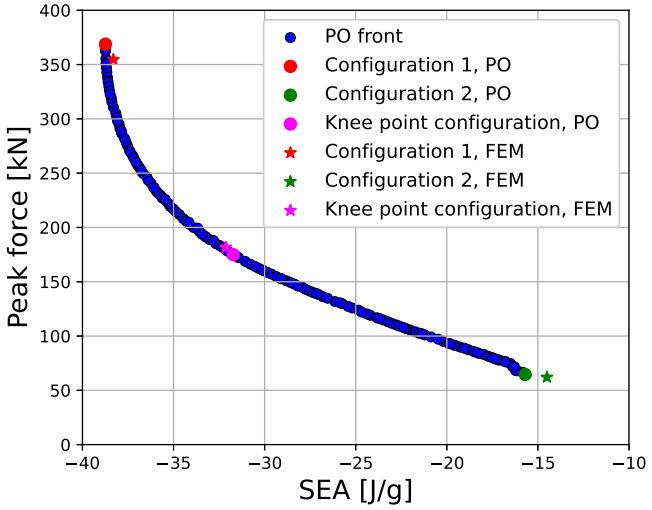

Fig. 16. PO and FEM results of selected geometry configurations.

not attainable in practice with presence of conflicting objectives. This minimum distance D is calculated after scaling the points of the Pareto set between 0 and 1 for both variables, using the following formula:

$$D = \min\left[\left(\sum_{i=i}^{d}\left(f_{ci} - \min\left(f_i(\mathbf{x})\right)\right)^d\right)^{\frac{1}{d}}\right] \tag{16}$$

where d is the number of the objective components, f_{ci} is the ith objective value in the cth Pareto solution and $\min(f_i(\mathbf{x}))$ represents the minimum value of all objective function values. The knee design point typically offers an overall optimal solution in the objective space, as it is regarded as a well-balanced compromise for conflicting and competing objectives [39].

These three configurations were also simulated using Abaqus/CAE. Results are shown in Fig. 16.

The four geometrical variables, the absorbed specific energy and maximum crushing force related to the three identified configurations are presented in Table 8, both for PO and FEM cases, with the response variables' relative errors highlighted. In order to have a meaningful crashworthiness performance parameters comparison, also EC4 FEM-obtained results and geometrical variables are reported in Table 8.

Fig. 17 displays the models generated in Abaqus/CAE, offering a clear view of the structural wall thicknesses, while Fig. 18 shows the deformation modes of the three optimized structures. Configuration 1 and the Knee Point configuration exhibit a global buckling mode, while Configuration 2 shows an non-symmetric mode of deformation, for which distortion of the part does not exhibit symmetry about any axis or plane [30].

The close alignment between the results produced by the NSGA-II genetic algorithm and those obtained through Finite Element Analysis underscores the utility of using this tool alongside FEM in the early design stages, yielding impressive outcomes. Adequate algorithm training substantially diminishes the computational resources required for structural optimization.

In order to gain a comprehensive understanding of the increased crashworthiness capabilities of these geometries, Abaqus/CAE simulations for three reference cylinders possessing equal masses to their respective optimized geometries were carried out.

The graphs in Fig. 19 depict the force–displacement curves of the optimized geometries and their respective reference cylinders, while Fig. 20 present the values of the response variables for both cases and their corresponding percentage variations.

The CFE, F_{max}, and SEA data presented in the figures were computed taking into account the compression of the structures up to a length of 20 mm.

As it can be observed from Fig. 19, all three optimized geometries significantly improve the properties of the baseline absorber while maintaining the same mass.

To delve into greater detail, Configuration 1 (Fig. 19(a)) exhibits a substantial improvement in all three crashworthiness parameters discussed. In this scenario, the increase in maximum force is not a concern, given the high crushing efficiency of the chosen geometry. Consequently, the accelerations transferred to a hypothetical occupant remain relatively constant, without significant peaks.

Conversely, Configuration 2 (Fig. 19(b)) offers a different form of improvement compared to Configuration 1. Although there is a minor increase in SEA, the most noteworthy enhancements lie in the significant rise in CFE and the reduction of maximum force during compression. This implies that the absorber's behaviour is closer to that of an ideal absorber, achieving nearly the same energy absorption of the baseline geometry while minimizing the risk of excessive occupant accelerations.

Regarding the Knee Point configuration (Fig. 19(c)), the considerations are akin to those made for Configuration 1. Nevertheless, it is of significant importance to highlight that this configuration seems to excel in combining the need for enhanced specific absorbed energy compared to a baseline geometry, which is similar to that of the first configuration, and the need to minimize the peak force, thereby enhancing overall efficiency. Notably, the percentage increase in the

Table 8
Structural parameters and optimized variables of selected configurations and of EC4.

	Configuration 1	Configuration 2	KP configuration	EC4
SEA (PO) [J/g]	38.74	15.69	32.35	–
SEA (FEM) [J/g]	38.31	14.50	32.14	32.50
R_e(SEA) [%]	1.13	8.21	0.65	–
Peak force (PO) [kN]	368.79	64.61	181.33	–
Peak force (FEM) [kN]	354.52	62.06	181.68	285.22
$R_e(F_{max})$ [%]	4.02	4.11	0.18	–
Wall thickness [mm]	1.0	1.0	1.0	2.55
Cylinder thickness [mm]	2.42	1.42	1.54	2.55
Cylinder radius [mm]	5.62	2.5	4.07	4.0
Amplitude parameter [–]	0.0	1.49	0.0	0.0
Mass [g]	164	84.6	101	157

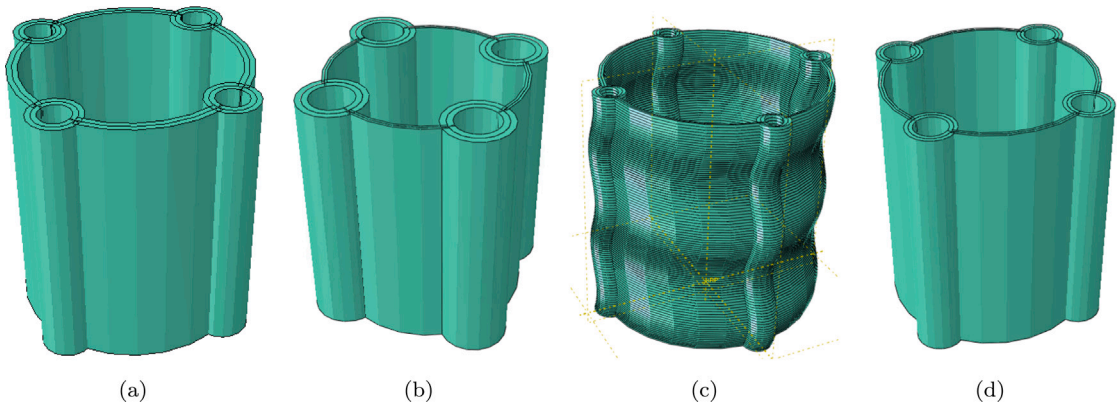

Fig. 17. (a) EC4 and optimal configurations' Abaqus models: (b) Configuration 1, (c) Configuration 2, (d) Knee Point configuration.

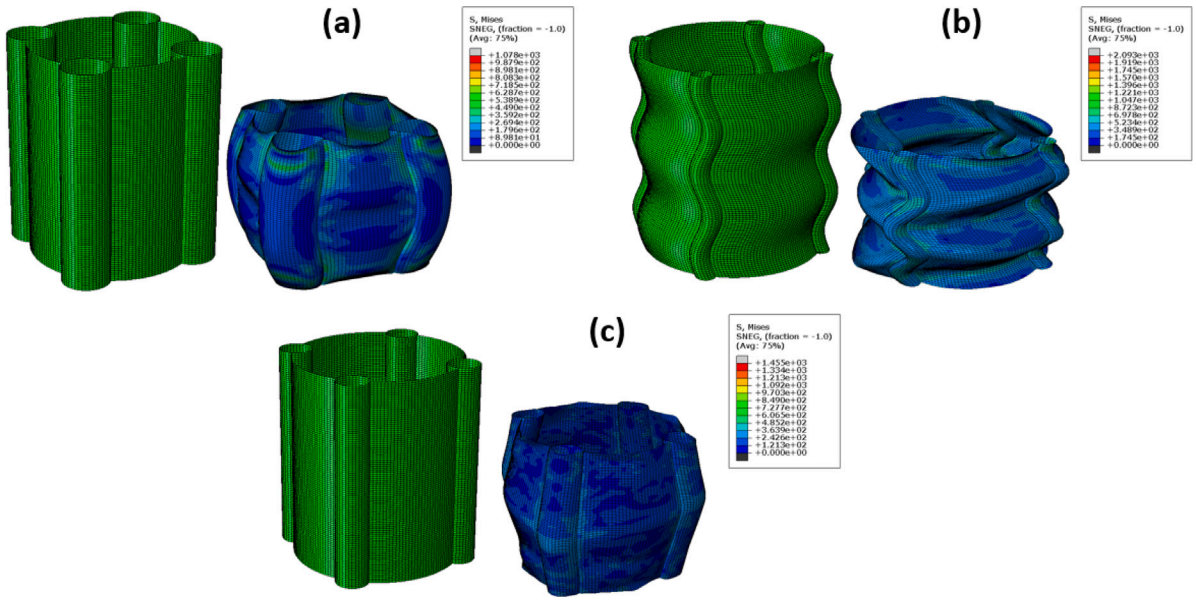

Fig. 18. Undeformed and deformed shapes of the three optimized structures: (a) Configuration 1, (b) Configuration 2, (c) Knee Point configuration.

maximum force is lower than that of the first configuration, while CFE is higher.

The EC4 geometry identified through the COPRAS methodology in Section 3.3 shows SEA and CFE values very similar to the Knee Point configuration (Fig. 20). However, the latter, besides having a lower peak of maximum force, has a mass almost half that of EC4. Moreover, the improvements of EC4 compared to the reference base geometry are generally lower than the three optimized geometries.

Furthermore, it is noteworthy that in all four cases, the optimized geometries lead to a substantial reduction in the force peaks associated with instability phenomena among the successive folds along the height of the structure. This phenomenon, which is frequently observed in metallic cylindrical absorbers, is indicative of regions experiencing high tensile and compressive forces. These regions signify the presence of structural segments that do not actively contribute to energy absorption and other areas that instead exhibit localized and pronounced deformation zones. Given that the absorber's primary objective is to effectively store the initial kinetic energy in a stable and controlled manner, a near constant force is more desirable than a force that fluctuates around a mean value [40].

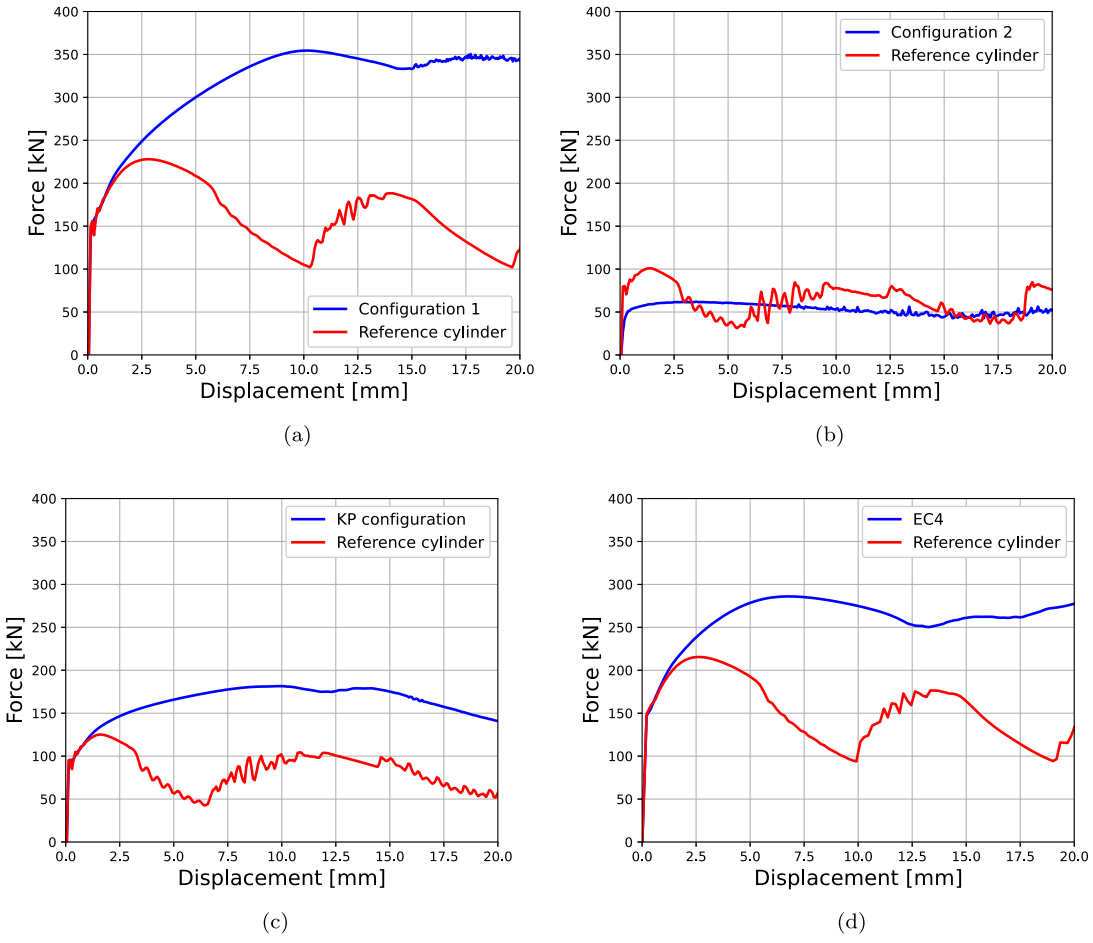

Fig. 19. Force–displacement curves comparison between EC4/selected optimized geometries and reference cylinders: (a) Configuration 1, (b) Configuration 2, (c) Knee Point configuration, (d) EC4.

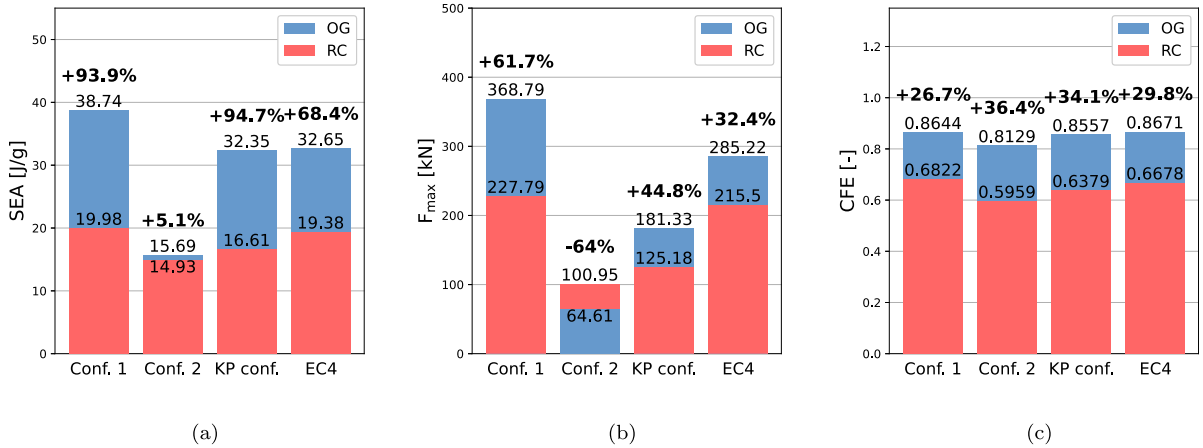

Fig. 20. Crashworthiness parameters comparison between EC4/selected optimized geometries (OG) and reference cylinders (RC) (a) SEA results, (b) F_{max} results, (c) CFE results.

These results clearly indicate a substantial improvement in all performance aspects when structures of equal mass are taken into account. Therefore, it is possible to affirm the multi-objective optimization using NSGA-II genetic algorithm, if the algorithm is properly trained, yield results that strongly agree to those of simulations in a finite element analysis. Furthermore, it also serves as a highly effective solution for structural optimization, particularly during the initial design phase.

6. Conclusions and further developments

In this study, optimization was carried out to improve the crashworthiness performance of bio-inspired sandwich core cell structures. SEA, $F_{\max}$, and CFE were considered as performance measures for crashworthiness, and they were calculated using Explicit Finite Element analysis. An elytra-inspired part, featuring four reinforcing cylinders (EC4), was

initially selected among other bamboo and elytra-inspired geometries through the COPRAS methodology. Response surface models for SEA and F_{max} were coupled with the genetic algorithm NSGA-II to find optimum design variables through multi-objective optimization. The radius of reinforcing cylinders, a sine wave parameter of an along-the-height deformation line, and cylinder and walls thicknesses were considered as design variables. A Pareto-Optimal front was obtained, from which three optimal configurations were identified: *Configuration 1*, which maximizes the SEA, shows a 93.9% increase in SEA with respect to a baseline hollow cylinder with the same mass; *Configuration 2*, which minimizes F_{max}, shows a decrease in F_{max} of 64% with respect to a baseline geometry, while still enhancing SEA and CFE; and the *Knee Point configuration*, determined using the minimum distance selection method, excels in combining the enhancement in SEA (+94.7%) and in CFE (+34.1%) and the minimization of F_{max} (only +26.7%).

In general, the use of NSGA-II as a multi-objective optimization algorithm in conjunction with FEM analysis for structural optimization has proven to be effective in an initial design phase. It yields to results that strongly agree to those of a finite element analysis and it significantly lowers the computational demand for optimization purposes. In conclusion, honeycomb 3D-printable structures designed through numerical optimization algorithms represent a promising frontier of innovation in engineering, with an interest that has grown enormously in recent years.

Future expansions of the work should address the design of a complete honeycomb panel to study bending effects and interactions among the structure's walls. The implementation of a genetic algorithm capable of accounting for more than two response variables may be interesting to discover even more high-performing structures.

CRediT authorship contribution statement

Bianca Omede': Writing – review & editing, Writing – original draft, Visualization, Validation, Software, Methodology, Investigation, Formal analysis, Data curation, Conceptualization. **Antonio Mattia Grande:** Writing – review & editing, Supervision, Project administration, Methodology, Conceptualization.

Declaration of competing interest

The authors declare that they have no known competing financial interests or personal relationships that could have appeared to influence the work reported in this paper.

Data availability

Data will be made available on request.

References

[1] N. San Ha, G. Lu, A review of recent research on bio-inspired structures and materials for energy absorption applications, Composites B 181 (2020) 107496.

[2] A.-G. Olabi, E. Morris, M. Hashmi, Metallic tube type energy absorbers: a synopsis, Thin-Walled Struct. 45 (7–8) (2007) 706–726.

[3] W. Zhang, J. Xu, T. Yu, Dynamic behaviors of bio-inspired structures: Design, mechanisms, and models, Eng. Struct. 265 (2022) 114490.

[4] K. Günaydın, Z. Eren, Z. Kazancı, F. Scarpa, A.M. Grande, H.S. Türkmen, In-plane compression behavior of anti-tetrachiral and re-entrant lattices, Smart Mater. Struct. 28 (11) (2019) 115028.

[5] F. Usta, Z. Eren, H. Kurtaran, H.S. Türkmen, Z. Kazancı, Z. Mecitoglu, Crashworthiness optimization of nested and concentric circular tubes using response surface methodology and genetic algorithm, Latin Am. J. Solids Struct. 15 (2018).

[6] A. Olabi, E. Morris, M. Hashmi, M. Gilchrist, Optimised design of nested circular tube energy absorbers under lateral impact loading, Int. J. Mech. Sci. 50 (1) (2008) 104–116.

[7] A.A. Nia, S. Chahardoli, Optimizing the layout of nested three-tube structures in quasi-static axial collapse, Thin-Walled Struct. 107 (2016) 169–181.

[8] N. San Ha, T.M. Pham, H. Hao, G. Lu, Energy absorption characteristics of bio-inspired hierarchical multi-cell square tubes under axial crushing, Int. J. Mech. Sci. 201 (2021) 106464.

[9] L. Meng, J. Zhao, X. Lan, H. Yang, Z. Wang, Multi-objective optimisation of bio-inspired lightweight sandwich structures based on selective laser melting, Virtual Phys. Prototyp. 15 (1) (2020) 106–119.

[10] N. San Ha, T.M. Pham, W. Chen, H. Hao, G. Lu, Crashworthiness analysis of bio-inspired fractal tree-like multi-cell circular tubes under axial crushing, Thin-Walled Struct. 169 (2021) 108315.

[11] N. San Ha, T.M. Pham, T.T. Tran, H. Hao, G. Lu, Mechanical properties and energy absorption of bio-inspired hierarchical circular honeycomb, Composites B 236 (2022) 109818.

[12] EPMA, Introduction to Additive Manufacturing Techonlogy, third ed., 2019.

[13] A. Ingrole, T.G. Aguirre, L. Fuller, S.W. Donahue, Bioinspired energy absorbing material designs using additive manufacturing, J. Mech. Behav. Biomed. Mater. 119 (2021) 104518.

[14] J. Xiang, J. Du, Energy absorption characteristics of bio-inspired honeycomb structure under axial impact loading, Mater. Sci. Eng. A 696 (2017) 283–289.

[15] X. Yu, X. Zhang, J. Chen, L. Pan, Y. Xu, Y. Fu, Experimental verification and optimization research on the energy absorption abilities of beetle elytron plate crash boxes, Mater. Res. Express 6 (11) (2019) 1165e2.

[16] P. Hao, J. Du, Energy absorption characteristics of bio-inspired honeycomb column thin-walled structure under impact loading, J. Mech. Behav. Biomed. Mater. 79 (2018) 301–308.

[17] M. Zou, S. Xu, C. Wei, H. Wang, Z. Liu, A bionic method for the crashworthiness design of thin-walled structures inspired by bamboo, Thin-Walled Struct. 101 (2016) 222–230.

[18] Y. Xiao, H. Yin, H. Fang, G. Wen, Crashworthiness design of horsetail-bionic thin-walled structures under axial dynamic loading, Int. J. Mech. Mater. Des. 12 (2016) 563–576.

[19] J. Fang, G. Sun, N. Qiu, N.H. Kim, Q. Li, On design optimization for structural crashworthiness and its state of the art, Struct. Multidiscip. Optim. 55 (2017) 1091–1119.

[20] B. Wilson, D. Cappelleri, T.W. Simpson, M. Frecker, Efficient Pareto frontier exploration using surrogate approximations, Opt. Eng. 2 (2001) 31–50.

[21] N. Qiu, Y. Gao, J. Fang, Z. Feng, G. Sun, Q. Li, Crashworthiness analysis and design of multi-cell hexagonal columns under multiple loading cases, Finite Elem. Anal. Des. 104 (2015) 89–101.

[22] F. Tarlochan, F. Samer, A. Hamouda, S. Ramesh, K. Khalid, Design of thin wall structures for energy absorption applications: Enhancement of crashworthiness due to axial and oblique impact forces, Thin-Walled Struct. 71 (2013) 7–17.

[23] A. Bigdeli, M.D. Nouri, A crushing analysis and multi-objective optimization of thin-walled five-cell structures, Thin-Walled Struct. 137 (2019) 1–18.

[24] M. Smith, ABAQUS/Standard User's Manual, Version 6.9, Dassault Systèmes Simulia Corp, United States, 2009.

[25] K. Kadam, N.S. Khan, Buckling analysis of thin walled cylinders subjected to axially compressive load by ANSYS, Int. J. Eng. Res. Technol. (IJERT) 2 (12) (2013) 1407–1413.

[26] E. Zavadskas, A. Kaklauskas, V. Šarka, The new method of multicriteria complex proportional assessment of projects, Technol. Econ. Dev. Econ. 1 (1994) 131–139.

[27] Y. Wu, Q. Liu, J. Fu, Q. Li, D. Hui, Dynamic crash responses of bio-inspired aluminum honeycomb sandwich structures with CFRP panels, Composites B 121 (2017) 122–133.

[28] B. Chen, M. Zou, G. Liu, J. Song, H. Wang, Experimental study on energy absorption of bionic tubes inspired by bamboo structures under axial crushing, Int. J. Impact Eng. 115 (2018) 48–57.

[29] J. Du, P. Hao, M. Liu, F. Scarpa, Multi-cell energy-absorbing structures with hollow columns inspired by the beetle elytra, J. Mater. Sci. 55 (10) (2020) 4279–4291.

[30] J. Legendre, P. Le Grognec, C. Doudard, S. Moyne, Analytical, numerical and experimental study of the plastic buckling behavior of thick cylindrical tubes under axial compression, Int. J. Mech. Sci. 156 (2019) 494–505.

[31] D.C. Montgomery, Design and Analysis of Experiments, John wiley & sons, 2017.

[32] R. Qin, J. Zhou, B. Chen, Crashworthiness design and multiobjective optimization for hexagon honeycomb structure with functionally graded thickness, Adv. Mater. Sci. Eng. 2019 (2019) 1–13.

[33] H. Yin, Y. Xiao, G. Wen, Q. Qing, X. Wu, Crushing analysis and multi-objective optimization design for bionic thin-walled structure, Mater. Des. 87 (2015) 825–834.

[34] K. Deb, A. Pratap, S. Agarwal, T. Meyarivan, A fast and elitist multiobjective genetic algorithm: NSGA-II, IEEE Trans. Evol. Comput. 6 (2) (2002) 182–197.

[35] Y. Zhang, G. Sun, G. Li, Z. Luo, Q. Li, Optimization of foam-filled bitubal structures for crashworthiness criteria, Mater. Des. 38 (2012) 99–109.

[36] J. Blank, K. Deb, Pymoo: Multi-objective optimization in python, IEEE Access 8 (2020) 89497–89509.

[37] J. Blank, K. Deb, A running performance metric and termination criterion for evaluating evolutionary multi-and many-objective optimization algorithms, in: 2020 IEEE Congress on Evolutionary Computation, CEC, IEEE, 2020, pp. 1–8.
[38] G. Sun, G. Li, S. Zhou, H. Li, S. Hou, Q. Li, Crashworthiness design of vehicle by using multiobjective robust optimization, Struct. Multidiscip. Optim. 44 (2011) 99–110.
[39] J. Branke, K. Deb, H. Dierolf, M. Osswald, Finding knees in multi-objective optimization, in: Parallel Problem Solving from Nature-PPSN VIII: 8th International Conference, Birmingham, UK, September 18-22, 2004. Proceedings 8, Springer, 2004, pp. 722–731.
[40] J. Marsolek, H.-G. Reimerdes, Energy absorption of metallic cylindrical shells with induced non-axisymmetric folding patterns, Int. J. Impact Eng. 30 (8–9) (2004) 1209–1223.